Variable-order modeling of nonlocal emergence in many-body systems: Application to radiative dispersion

J. Orosco and C. F. M. Coimbra*

Department of Mechanical and Aerospace Engineering, Center for Energy Research, University of California San Diego, La Jolla, California 92093-0411, USA

(Received 12 July 2018; published 13 September 2018)

We describe a physical framework for analyzing the spectral dynamics of a broad range of media. The framework is built on a variable-order calculus formalism that permits the description of temporally nonlocal behavior. Such emergent behavior is observed in the response of assorted complex media. The analytical features of the formalism are discussed and it is demonstrated how they correspond to the generalization of other well known theories for the description of nonlocal many-body effects. The framework is employed to analyze a set of spectroscopic data for the high-frequency dielectric response of a nanofluidic graphene dispersion and the midinfrared optical response of amorphous quartz silica. A practical application of the analysis is facilitated by a model definition that generalizes the semiclassical Lorentz theory to allow for nonlocal damping effects. The model is derived from a fractional order differential equation of motion. From the analysis, an estimated parametrization for the model structure is obtained. The fidelity of the analysis methodology is validated against optimized parametrizations in a multiobjective (optical and radiative) setting. The results demonstrate the utility of the analysis and indicate a specific well-defined region of nonlocality having a distinct fidelity that encompasses the entire Pareto front. This region is shown to be inaccessible to integer order descriptions of the mean field dynamics.

DOI: 10.1103/PhysRevE.98.032208

I. INTRODUCTION

The earliest contributions to applied fractional calculus were made by Heaviside [1]. Since that time, the analysis of systems having complex constitutive relations has greatly benefited from models based on noninteger differintegral operators. Due to the availability of data produced by increasingly accurate experimentation, along with the parallel development of the nonlocal (i.e., noninteger order) theoretical models, numerous studies have provided empirical verification of nonlocal dynamics. Among the many diverse areas employing such methods, a few are fluid mechanics, radiative mechanics, rheology, electrochemistry, solid state physics, biomechanics, and geophysics [2–11].

Variable order operators are those possessing a functionally dependent operator order. The earliest research related to variable-order calculus was performed mainly from a mathematical viewpoint [12–14], while more recent contributions have focused on the development of a consistent physical theory [15,16]. Models utilizing variable-order operators have been employed to describe elastomeric strain [17], advective-dispersive systems [18], particulate flows [19,20], and for the analysis of the stability characteristics of variable damping regimes in a closed loop setting [21]. Previous studies involving variable-order operators have taken place, almost without exception, in the time domain.

In this work, we develop a variable-order framework for the analysis and physical interpretation of complex systems in the frequency domain. The framework is used to analyze systems originating from integer order differential equations as well as those exhibiting features that are well modeled by temporally nonlocal response equations. We apply this framework specifically to spectroscopic data. To facilitate the application of the variable-order framework, we also define a nonlocal dispersion model that generalizes the semiclassical Lorentz theory. The model is motivated by the stochastic nature of the long-range structure in amorphous media and the success of nonlocal operators at reproducing the emergent effects of many-body dynamics [22,23].

The organization of this work is as follows: in Sec. II we briefly review the fundamentals of material response theory and define the relevant variable-order nonlocal differential and integral operators. In Sec. III we introduce the harmonic oscillator models referenced in this work. In particular, Sec. III B introduces the nonlocal dispersion model, considers its physical interpretations, and discusses its physical consistency. In Sec. IV the variable-order frequency domain analysis framework is derived and its analytical features are delineated. An application of the analysis framework is demonstrated in Sec. V, where it is used to obtain a parametrization for the previously noted dispersion model on experimental data. The results are then compared against those obtained via optimization. Section VI consists of a brief concluding discussion.

II. THEORETICAL PRELIMINARIES

A. Response theory

The bulk macroscopic response of a material to electromagnetic forcing is described in the frequency domain by

*ccoimbra@ucsd.edu

 ©2018 American Physical Society

its relative permittivity (also, dielectric function), ε. Over absorptive bands, the permittivity is frequency-dependent and complex-valued (to account for phase loss). The permittivity of a medium having K distinct absorptive mechanisms in response to low-intensity forcing may be written [24]

$$\varepsilon(\nu) = \varepsilon_\infty + \sum_{k=1}^{K} \chi_k(\nu), \tag{1}$$

where ε_∞ is the core polarizability and where χ_k are the susceptibility contributions. In this work, we use ν interchangeably to denote wave number and frequency, taking care where necessary to specify the corresponding units.

When discussing optical properties, the complex permittivity is related to the complex refractive index:

$$\varepsilon' = n^2 - k^2, \tag{2a}$$

$$\varepsilon'' = 2\,n\,k, \tag{2b}$$

where n is the dispersive (real) index and k is the absorptive (imaginary) index, and where we have made use of the notational convention that $z' = \mathbb{R}\mathrm{e}\{z\}$ and $z'' = \mathbb{I}\mathrm{m}\{z\}$. The sign convention observed by the models in this work are such that $\varepsilon = \varepsilon' - i\,\varepsilon''$ and $\widetilde{n} = n - i\,k$, with $i = \sqrt{-1}$. The absorptive-dispersive indices can be used along with Fresnel's well-known equations to obtain many useful radiative and optical properties.

B. Operator definitions

The derivative definitions we will use all represent special cases of the definition originally proposed by Coimbra for differentiation to variable order $q(t) < M$, which is most generally expressed as [15,25]

$${}_*\mathcal{D}^{q(t)}x(t) = \int_{t_{0^+}}^{t} \frac{(t-\sigma)^{M-1-q(t)}}{\Gamma[M-q(t)]}\,\mathcal{D}^M x(\sigma)\,d\sigma + \sum_{m=0}^{M-1} \frac{[\mathcal{D}^m x(t_{0^+}) - \mathcal{D}^m x(t_{0^-})]\,t^{m-q(t)}}{\Gamma[m+1-q(t)]}, \tag{3}$$

where $\Gamma(\cdot)$ is the gamma (generalized factorial) function, $M = \lceil q(t) \rceil$ with $\lceil\cdot\rceil$ being the ceiling operator, and where we use the operator notation $\mathcal{D}^{(\cdot)}$ to represent differentiation of order $(\cdot)$ with respect to time. For the sake of mathematical clarity, we denote constant noninteger orders with μ and variable orders with $q(\cdot)$. The interested reader can refer to the Appendix for the most generic definition of the operator. Coimbra and co-authors have previously shown that an appropriately weighted sum of interpolating fractional derivatives converges to the foregoing definition as the number of interpolating terms is increased [26]. Under a requisite set of physical and mathematical criteria, it has also been previously established that this definition is the appropriate choice when modeling dynamical systems [16].

The physical meaning of the summation on the right-hand side of (3) is embedded in the fact that it evaluates to zero only if the system is in equilibrium for all times $t \in (-\infty, 0^+]$. This is necessary since the path-dependent memory of nonlocal systems decays asymptotically, so that the system can only initialize from a true zero-memory state if it has been in equilibrium for all times previous. Under an approximate assumption of thermodynamic equilibrium (appropriate for the macroscopic approach taken for modeling the statistical mechanical systems investigated here), we will assume this sum is zero throughout.

When equations of motion for the variable $x(t)$ have a stationary long-time response, both q and x generally become frequency dependent, and one may write the stationary Laplace transform

$$\mathcal{L}\{{}_*\mathcal{D}^{q(t,p)}x(t)\} = s^{\overline{q}(\nu,p)}\hat{x}(s), \tag{4}$$

where s is the Laplace parameter resulting from the transform $\mathcal{L}\{\cdot\}$, $\hat{x}$ is the transform of x, $\overline{q} = \lim_{t\to\infty} q$, and p has been used to denote the fact that q may generally depend on other (time-invariant) parameters. Within the context of the discussion to follow, condition (4) applies when the particle described by x has reached an energy eigenstate.

For inversion of a variable-order Laplace expression, we define the Riemann-Liouville-type integral of (frequency-dependent) order $q(\nu) > 0$:

$$\mathcal{I}^{q(\nu)}x(t) = \int_{t_0}^{t} \frac{(t-\sigma)^{q(\nu)-1}}{\Gamma[q(\nu)]}\,x(\sigma)\,d\sigma. \tag{5}$$

III. HARMONIC OSCILLATOR MODELS

A. Complex damped harmonic oscillator

In well-ordered lattice configurations at nominal temperatures, the mean field particle dynamics of solid dielectric media can be reasonably expected to follow a spatially local response. This consideration, for example, underlies the prevalence of the Born–von Karman (periodic) boundary conditions often employed to simplify the analyses found in many standard statistical physics texts [27,28]. The complex damped harmonic oscillator (CDHO)—also known as the Lorentz oscillator—is a natural extension of this concept into the realm of macroscopic, phenomenological susceptibility models.

In the time domain, the CDHO represents a susceptibility model for bound particle oscillations that treats the mean field response from the viewpoint of a the spatially localized behavior of an individual particle whose dynamics are governed by the second-order displacement ODE [29]:

$$\mathcal{D}^2 x(t) + \gamma\,\mathcal{D}^1 x(t) + \nu_n^2\,\mathcal{D}^0 x(t) = F(t;\nu), \tag{6}$$

where the undamped natural frequency, $\nu_n = \sqrt{\kappa/m}$, is determined by the particle mass m and the binding stiffness κ, and $F(t;\nu) = (-e/m)\,E(t;\nu) = (-e\,E_0/m)\,\mathbb{R}\mathrm{e}\{\exp(i\,\nu\,t)\}$ is the electromagnetic forcing (applied to a particle of charge e) due to incident radiation having a wavelength $\lambda = 2\pi/\nu$. With respect to, e.g., the phononic infrared response of dielectric media, the damping corresponds to a quasiparticle lifetime of $\tau = 1/\gamma$. The statistical correlations of the microscopic CDHO under a Langevin description have been recently investigated [30]. The noted study also includes an interesting analysis of the microscopic oscillator energy correlations.

By relating the bulk volumetric polarization to the individual dipole displacement and then applying a stationary Laplace transform, one obtains the traditional form of the

CDHO,

$$\chi^L(\nu) = \frac{\nu_p^2}{\nu_n^2 - \nu^2 + i\,\gamma\,\nu}, \tag{7}$$

where the plasma frequency $\nu_p = \sqrt{4\pi\, n_d\, e^2/m}$ is related to the number density, n_d, of the particles in the medium. An important takeaway from this model is that the damping, as expressed in (6) and (7), is assumed to be linearly proportional to the instantaneous particle (or dipole) displacement velocity and results from the interaction of the particle with a well ordered local field.

B. Complex μ-damped harmonic oscillator

In amorphous media, we expect the behavior to deviate from the classical theory due to long range structural stochasticity [31], which may impart a historical path dependence on the constituent behavior at a given time. Since this will arise from locally exerted forces, we model this in terms of its net effect on the constituent lifetime. In the case of condensed media, we postulate that the particle lifetime in a disordered lattice arises by the same mechanisms assumed in the classical theory, except where now they may depend on previous excited states.

The notion of non-Markovian macroscopically emergent timescale mixing arising due to stochastic microscopic dynamics has been studied within statistical mechanical framework by generalizing the method of Van Hove [22,23]. In these works it was demonstrated that the appropriate mathematical formalism for such a phenomenological description is the fractional calculus. In keeping with the foregoing postulate, we define the complex μ-damped harmonic oscillator (which we denote CD$^\mu$HO) in terms of the second-order fractional displacement ODE:

$$\mathcal{D}^2 x(t) + \gamma_\mu^{2-\mu}\,\mathcal{D}^\mu x(t) + \nu_\mu^2\,\mathcal{D}^0 x(t) = F(t;\nu), \tag{8}$$

where $\mu > 0$ may be interpreted in the time domain as indicating the extent of the memory of the particle of its prior states. That is, when $\mu = 1$, the classical theory is recovered and the particle is said to be "perfectly forgetful" (i.e., it depends only on the *instantaneous* displacement velocity). When $\mu \neq 1$, the particle's behavior at a given instant depends on a decaying memory of the net damping resulting from previous local field interactions. In Ref. [32], Burov gives an excellent thorough analysis of the statistical properties of the microscopic CD$^\mu$HO under a Langevin description (along with other related oscillators).

If we consider the stationary response of the system (i.e., when transient memory effects and memory of the initial conditions have both vanished), then the corresponding susceptibility model is obtained by Laplace transform [33]:

$$\chi^\mu(\nu) = \frac{\nu_p^2}{\nu_\mu^2 - \nu^2 + \gamma_\mu^{2-\mu}(i\,\nu)^\mu}. \tag{9}$$

Some intuition about the nature of the fractional damping term can be achieved by noting that in a Hamiltonian description of a closed system, dissipation is modeled by coupling the particle to a bath that absorbs the dissipated energy [29]. Then the bath represents the net effect of N-body dynamics on the particle and the observed damping *emerges* as a net effect of the many-body conservative dynamics.

Accordingly, the fractional damping term can be understood as phenomenologically modeling the net damping effect of a potentially non-Markovian bath imposed by the lattice disorder. More rigorous treatments of this idea do, in fact, lead to equations of motion coupled to a history integral over the interacting bath [34,35]. This interpretation is also in agreement with the common use of fractional operators for modeling many-body dynamics. Indeed, Jonscher has previously posited—in developing his renowned "universal dielectric response" theory—that the power-law (i.e., fractional) frequency dependence observed in many materials at sub-GHz frequencies arises from the relatively slow adjustment of the many-body background field to the fast hopping electrons or dipoles [36]. This description bears a remarkable similarity to that of the Basset history drag, which arises in fluid mechanical models of the motion of a spherical particle in, e.g., high-frequency harmonic Stokes flows [4,37]. The Basset term is proportional to a nonlocal derivative of order $1/2$. It is also worth noting that the stretched-exponential attenuation of radiation empirically observed in certain random media has been successfully modeled using space-fractional generalizations of the corresponding integer order theoretical frameworks (e.g., Beer's Law) [6,38].

Note that if we choose to neglect the inertial effects in our fractional displacement ODE model (as is usually done when modeling, e.g., polymer solution dynamics), then the corresponding susceptibility model can be expressed as

$$\chi^{CC}(\nu) = \frac{\varepsilon_0 - \varepsilon_\infty}{1 + (i\,\nu\,\tau)^{1-\alpha}}, \tag{10}$$

where $\varepsilon^{CC}(\nu) = \varepsilon_\infty + \chi^{CC}(\nu)$ is the well-known Cole-Cole equation describing the dielectric response of the medium [39]. The Cole-Cole equation serves the purpose of generalizing to fractional order the classical Debye model, which is recovered by setting $\alpha = 0$ in (10). Then (9) may also be interpreted as extending the Cole-Cole description for use with systems where the inertial effects play an important role.

1. Model properties

One must take care when modeling in the frequency domain to ensure that a particular response model defines a subset of all materials that can exist in nature. For this purpose, we appeal to the Kramers-Kronig relations (KKRs) [40–42]. KKR consistency can be confirmed by verifying [43]: (i) that the model is analytic in the closed upper half complex plane and (ii) that the model is Hermitian.

It is well known that the CDHO is KKR compliant. It can be shown by a direct (albeit lengthy) application of the Cauchy-Riemann equations [44] that item 1 above holds for the CD$^\mu$HO as long as $\gamma > 0$ (i.e., the system must be dissipative for all $\nu > 0$) and $0 < \mu < 2$. Note that enforcing the strict limits in the latter requirement also ensures that expression (9) has a nonzero dissipative component for all ν. The Hermicity requirement is proved by showing that $\overline{\chi^\mu(\nu)} = \chi^\mu(-\nu)$, where $\overline{z}$ is the complex conjugate of z.

A secondary check on the physical consistency of susceptibility models of the type proposed here is to verify adherence

to a relevant sum rule. For this purpose, we define the energy absorption measure on a frequency domain response model $\chi = \chi' - i\,\chi''$ as

$$\mathcal{A}[\chi] = \int_0^\infty \nu\,\chi''(\nu)\,d\nu. \tag{11}$$

By separating the real and imaginary parts of (9), defining $\rho(\nu) = \rho'(\nu) + i\,\rho''(\nu)$, and then writing

$$\chi^\mu(\nu) = \nu_p^2\left[\frac{\rho'(\nu)}{|\rho(\nu)|^2} - i\,\frac{\rho''(\nu)}{|\rho(\nu)|^2}\right], \tag{12}$$

where we have also defined

$$\rho'(\nu) = \nu_\mu^2 - \nu^2 + \gamma_\mu^{2-\mu}\nu^\mu\cos\left(\frac{\pi\,\mu}{2}\right), \tag{13a}$$

$$\rho''(\nu) = \gamma_\mu^{2-\mu}\nu^\mu\cos\left(\frac{\pi\,\mu}{2}\right), \tag{13b}$$

it is made immediately apparent that above some frequency $\nu_h \gg \nu_\mu$ we have $\mathbb{R}\mathrm{e}\{\chi^\mu\} \approx -\nu_p^2/\nu^2$. By combining this result with the KKR consistency of the model, it can be directly shown that

$$\mathcal{A}[\chi^\mu] = \tfrac{1}{2}\pi\,\nu_p^2, \tag{14}$$

so that the CD$^\mu$HO adheres to the well-known plasma sum rule [45].

2. Energetic interpretation

An important interpretation is obtained by noting that the expressions (13) represent complimentary partitions of the oscillator energy into dispersive (conservative) (13a) and absorptive (dissipative) (13b) components. The role of μ in these expressions is to provide a tunable coupling between the two partitions, a feature that is absent from the CDHO. In the section that follows, we formalize this idea of energetic partitioning by deriving a generalized dynamic analysis framework. Doing so requires adopting a more general differential operator definition that permits a continuously variable order. The resulting analytical tools are quite general and can be used for integer order differential equations, as well as for their fractional and variable-order counterparts.

IV. VARIABLE ORDER FORMALISM

In the framework that follows, the variable-order parameters are shown to constitute a mathematical basis for the complex plane—which we regard as being the entire space over which the system's dynamics may be defined (henceforth referred to simply as the "dynamic space")—and are used to describe complex-valued trajectories that represent the subset of the dynamic space correlated to the actual system dynamics. Within this context, we refer to the variable-order parameters as variable-order coordinates (VOCs) for reasons that will be presently made clear and we refer to the general analysis framework as the variable-order formalism (VOF).

As will be demonstrated presently, the VOF represents a generalized macroscopic description of the system as an energetic reservoir that either absorbs or rejects energy. This is analogous to dynamic mechanical analysis. Its distinctiveness lies in the fact that it is based on a continuously variable derivative order, so that the description of the energetic evolution as a function of forcing frequency can account for nonlocal dynamics. Such dynamics often arise as a result of many-body dynamics, so that this framework is particularly well suited for the analysis of spectroscopic systems.

A. Physical origin of the VOF

Consider a simple viscoelastic oscillator described by the fractional second-order displacement ordinary differential equation (FODE)

$$m\,\mathcal{D}^2x(t) + c\,{}_*\mathcal{D}^{1/2}x(t) + k\mathcal{D}^0x(t) = F(t), \tag{15}$$

where x is the position, F is the forcing, m is the mass, c is the viscoelastic damping coefficient, and k is the binding stiffness. Allowing for multiple fractional damping orders μ_n that may be either viscoelastic $\mu \in (0, 1)$ or viscoinertial $\mu \in (1, 2)$, a generalized FODE may be written

$$\sum_{n=0}^{N}\gamma_n\,{}_*\mathcal{D}^{\mu_n}x(t) = F(t), \tag{16}$$

where γ_n are generalized damping coefficients, and $\mu_0 = 0$ and $\mu_N = 2$. The corresponding stationary Laplace transform for constant fractional differentiation orders yields [33]

$$\frac{\hat{x}(s)}{\hat{F}(s)} = \sum_{n=0}^{N}\gamma_n s^{\mu_n}, \equiv G^{-1}(s). \tag{17}$$

Letting $s = i\,\nu$ with $i = \sqrt{-1}$, and then separating the real and imaginary parts leads to

$$\begin{aligned}\mathbb{I}\mathrm{m}\{G^{-1}(\nu)\} &= \sum_{n=0}^{N}\gamma_n\,\nu^{\mu_n}\sin\left(\frac{\pi\,\mu_n}{2}\right),\\ &= \sum_{n=1}^{N-1}\gamma_n\,\nu^{\mu_n}\sin\left(\frac{\pi\,\mu_n}{2}\right),\end{aligned} \tag{18}$$

where the latter equality is a result of the fact that $\sin(0) = \sin(\pi) = 0$. If $\mu_k = 1$ so that $\cos(\pi\,\mu_k/2) = 0$, then the real part is

$$\begin{aligned}\mathbb{R}\mathrm{e}\{G^{-1}(\nu)\} &= \sum_{n=0}^{N}\gamma_n\,\nu^{\mu_n}\cos\left(\frac{\pi\,\mu_n}{2}\right)\\ &= \sum_{n=0}^{k-1}\gamma_n\,\nu^{\mu_n}\cos\left(\frac{\pi\,\mu_n}{2}\right)\\ &\quad + \sum_{n=k+1}^{N}\gamma_n\,\nu^{\mu_n}\cos\left(\frac{\pi\,\mu_n}{2}\right).\end{aligned} \tag{19}$$

Given an M-sized set of frequency domain data (such as that obtained from experimental investigations of the optical properties of solid media) $Z_m \equiv Z(\nu_m)$, $m \in [1, M] \subset \mathbb{Z}_+$, it is natural to establish the relations

$$\sum_{n=0}^{N}\gamma_n\,\nu_m^{\mu_n}\sin\left(\frac{\pi\,\mu_n}{2}\right) = z_{i,m}, \tag{20a}$$

$$\sum_{n=0}^{N}\gamma_n\,\nu_m^{\mu_n}\cos\left(\frac{\pi\,\mu_n}{2}\right) = z_{r,m}, \tag{20b}$$

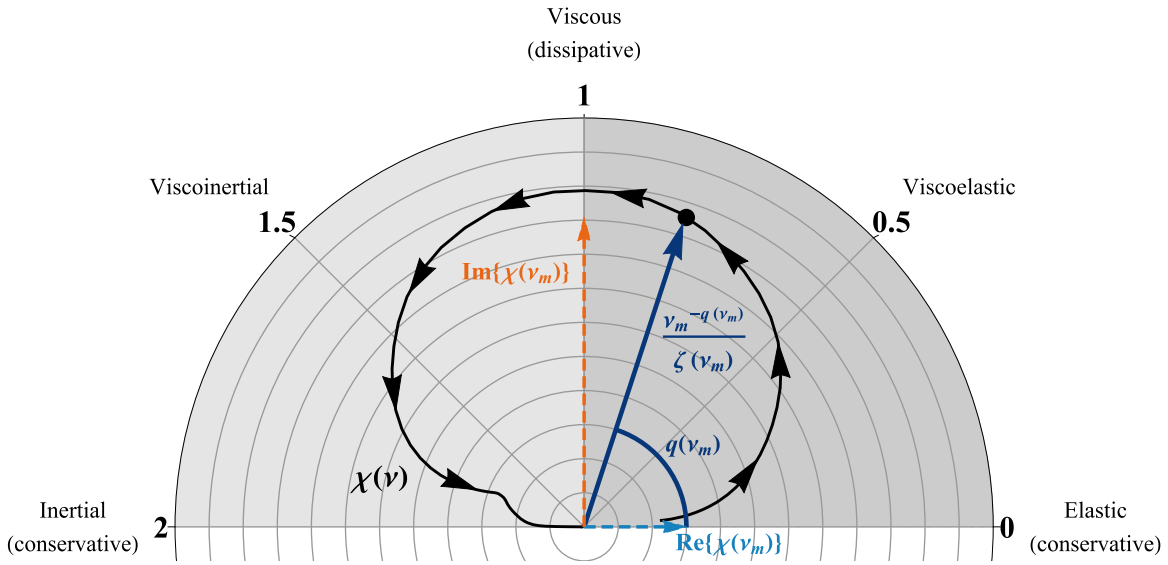

FIG. 1. The variable-order coordinates diagram for the midwavelength infrared susceptibility of amorphous quartz silica (SiO_2). The data are taken from Refs. [46,47]. The black curvilinear path traces out the trajectory of the dynamics $\chi(\nu)$ through the viscoelastic (dark gray region) and viscoinertial (light gray region) regimes, with arrowheads indicating direction of increasing frequency. The black dot indicates $\chi(\nu_m)$ where $\nu_m \approx 1040\ \mathrm{cm}^{-1}$, with angular component $q(\nu_m)$ defining the generalized differential order at ν_m. The dashed arrows, defined by the expressions (21), indicate the dissipative (imaginary, vertical) and conservative (real, horizontal) components of the system at ν_m, which represent orthogonal decompositions (or more precisely, phasor projections) of the "total" dynamics (indicated by the solid arrow). In the VOC diagram, the largest resonant mode is always the farthest point on the trajectory from the origin of the plot—in this case, the point at the top of the trajectory intersecting the dissipative axis $q = 1$.

where $z_{i,m}$ and $z_{r,m}$ are the imaginary (dissipative) and real (conservative) parts of Z_m (the dynamics), respectively. Typically, one sets, e.g., $Z_m = 1/\chi_m$, so that Z_m is directly associated with the system dynamics. Thus the equations are collocated on the frequency grid ν_m defined by the experimental data and coupled by the damping coefficients γ_n.

We are interested in a *variable* order description of the data, which can be obtained by replacing the constant order parameters $\{\gamma_n, \mu_n\}$ in (20) with parameters that vary freely with frequency $\{\zeta_m, q_m\}$. This leads to variable-order relations

$$\zeta_m\, \nu_m^{q_m} \sin\left(\frac{\pi\, q_m}{2}\right) = z_{i,m}, \tag{21a}$$

$$\zeta_m\, \nu_m^{q_m} \cos\left(\frac{\pi\, q_m}{2}\right) = z_{r,m}, \tag{21b}$$

where $q_m = q(\nu_m)$ are the variable derivative orders and $\zeta_m = \zeta(\nu_m)$ are the variable generalized damping coefficients, referred to jointly as the VOCs. Introducing the VOCs constitutes transforming a linear system of $2N + 2$ unknowns in two equations at each of M data points into a nonlinear system of two equations in two unknowns at each of M data points. The VOCs can be solved for explicitly at each ν_m:

$$q_m = \frac{2}{\pi} \operatorname{atan2}(Z_m), \tag{22a}$$

$$\zeta_m = \frac{1}{\nu_m^{q_m}} |Z_m|, \tag{22b}$$

where $|\cdot|$ is the complex modulus and with atan2$(\cdot)$ representing the phase-sensitive arctangent function. The VOCs are well defined for all inputs $Z_m \in \mathbb{C}$ and all frequencies $\nu_m > 0$.

If we let the VOCs be continuously defined as $\{\widetilde{\zeta}, \widetilde{q}\}$, then the VOF takes the form of a variable-order transfer function:

$$\widetilde{G}^{-1}(s) = \widetilde{\zeta}(\nu) s^{\widetilde{q}(\nu)}. \tag{23}$$

This provides a single-term basis for the entire dynamic space. It can be used to give insight into the energetic evolution of dynamical systems in relation to the differential order of the system. Before proceeding, we note that the expressions in (20) and (21) represent generalizations of dynamic moduli. Dynamic moduli are used in the discipline of dynamical system analysis (also, dynamic mechanical spectroscopy) to describe the energetic characteristics of a system as a function of forcing periodicity. They are orthogonal decompositions of the systemic energy into imaginary (dissipative) and real (conservative) components.

Bearing all of this in mind, the VOF is perhaps best understood by plotting the real and imaginary parts of the system response G as a contour, parameterized by frequency, and represented in the VOCs. Figure 1 shows the complex susceptibility $G = \chi$ for the midinfrared band of amorphous quartz silica (SiO_2), which is the subject of modeling efforts undertaken in later sections of this work. The ellipsometric data—resulting from the study of Ref. [46] and obtained in tabulated form from Ref. [47]—are plotted in a variable-order coordinates (polar) diagram, which makes it clear why the VOCs were so named. The figure shows how the dynamics of the system traverse the viscoelastic and viscoinertial regimes for increasing forcing frequencies (i.e., decreasing wavelengths). At any point in the trajectory of the system, the dynamics can be orthogonally decomposed into their

conservative and dissipative components, corresponding to the generalized dynamic moduli (21).

A wealth of information can be obtained from the variable-order coordinates diagram. For example, it is immediately apparent that no less than two linearly independent basis integer order differential operators (0 and 1 or 1 and 2) are needed in order to reach a given point in the dynamic space. This is because the order 0 (Hooke's law) and order 2 (Newton's law) operators can only reach disjoint portions of the conservative axis. Assigning damping coefficients to each operator then determines uniquely the trajectory taken by a given system as it traverses the space. In the absence of an order 2 operator (as in the previously noted polymer solution systems), the viscoinertial regime is entirely unreachable. This tells us, for example, that the Cole-Cole equation can only reach the viscoelastic regime, and is therefore not apt for describing modal dynamics that traverse the viscoinertial regime. It is also apparent that only a single appropriately chosen basis fractional order differential operator is needed to reach a given point in the space, and that with two such operators it is possible to construct a trajectory that traverses both the viscoelastic and viscoinertial regimes. Here it is important to recall that the terms "viscoelastic" and "viscoinertial" refer, in this context, to the type of energetic partitioning. In the time domain, these refer to the operative memory mechanism, with the former implying a positional memory and the latter implying a momentum memory.

Accordingly, and through the study of Fig. 1, it is made apparent why nonlocal operators should find utility in describing the dynamics of many-bodied systems. In these systems it is expected that nonlocal effects will play a more prominent role than in, e.g., systems well described by rigid-body dynamics, whose equations of motion are often derived directly from principles of Newtonian mechanics. As opposed to their integer order counterparts, nonlocal operators are capable of interpolating conservative and dissipative dynamics directly, rather than by superposition alone (as must be done with integer order operators). Accordingly, one may interpret the variable order q at any point in the system trajectory as the "bulk" or "macroscopic" differential order of the system. In this work, we will refer to q as the generalized differential order and to ζ as the generalized damping.

B. Relation to Jonscher's universal dielectric response

Many common systems, whether by topological scale similarity (i.e., "fractal topology") [48] or by some other mechanism [49], attain an approximately constant nonlocal emergent behavior over a given band. Jonscher noted this in his landmark study encompassing a broad range of material types, prompting him to write down his universal dielectric response (which he attributed directly to many-body dynamics), defined in Ref. [36] as

$$\frac{\chi''(\nu)}{\chi'(\nu)} = \cot\left(\frac{\pi\, n}{2}\right) = \frac{\text{energy lost per radian}}{\text{energy stored per radian}} = \text{const}, \tag{24}$$

where n is a real number. If we set $q = 1/n$ and solve for q in (24), then it is immediately clear that $q(\nu) = \mu = 1/n$ corresponds directly to constant fractional differential behavior along some band, as indicated by the VOF in (22a).

C. Relation to stationary radiative forcing

The model presented in (22) and (23) is directly related to the time domain stationary variable-order model given by Ramirez and Coimbra [16], with the notable exception that—as allowed and defined by the data—the VOCs in this frequency domain implementation vary continuously as a function of the frequency-dependent data. This type of analysis is directly applicable to the sinusoidal forcing imposed on solid media by incident electromagnetic radiation. For the reader's benefit, we summarize concisely the pertinent results of [16] within the context of the present discussion. Given a general fractional second-order system of the form

$$m\,\mathcal{D}^2 x(t) + c\,\mathcal{D}^1 x(t) + \sum_{n=1}^{N} \gamma_n\, {}_*\mathcal{D}^{\mu_n} x(t) + k\,\mathcal{D}^0 x(t) = F(t), \tag{25}$$

with radiative forcing $F(t) = E_0\,\mathbb{R}\text{e}\{e^{i\,\nu\,t}\}$ and where $\mu_n \in (0,1)\cup(1,2)$, we seek a single-term, variable-order model for its stationary behavior. The stationary variable-order derivative is given in terms of (3) as

$$\lim_{t_{0^+}\downarrow -\infty} {}_*\mathcal{D}^{q(t)} x(t) = \mathcal{D}^{q(\nu,\,p_q)} x(t), \tag{26}$$

where the set of variables p_q represent as-of-yet undetermined dependencies, so that, with the inclusion of variable damping ζ and assuming a sinusoidal steady-state response, we have

$$\begin{aligned}&\zeta(\nu,\,p_\zeta)\,{}_*\mathcal{D}^{q(\nu,\,p_q)} A\, e^{i\,\nu\,t} \\ &\quad = \left(m\,\mathcal{D}^2 + c\,\mathcal{D}^1 + \sum_{n=1}^{N} \gamma_n\, {}_*\mathcal{D}^{\mu_n} + k\,\mathcal{D}^0\right) A\, e^{i\,\nu\,t},\end{aligned} \tag{27}$$

with p_ζ defined in a fashion similar to p_q. Evaluating derivatives on both sides and dividing out common factors leads to

$$\zeta(\nu,\,p_\zeta)(i\,\nu)^{q(\nu,\,p_q)} = -m\,\nu^2 + c\,\nu + \sum_{n=1}^{N} \gamma_n\,(i\,\nu)^{\mu_n} + k. \tag{28}$$

Solving as in the VOF derivation, one obtains for the time domain stationary variable-order parameters

$$q(\nu,\,p_q) = \frac{2}{\pi}\text{atan2}(d_i,\,d_r) \tag{29}$$

and

$$\zeta(\nu,\,p_\zeta) = \frac{1}{\nu^{q(\nu,\,p_q)}}\sqrt{d_i^2 + d_r^2}, \tag{30}$$

where

$$d_i = c\,\nu + \sum_{n=1}^{N} \gamma_n\,\nu^{\mu_n} \sin\left(\frac{\pi\,\mu_n}{2}\right), \tag{31}$$

and

$$d_r = -m\,\nu^2 + \sum_{n=1}^{N} \gamma_n\,\nu^{\mu_n} \cos\left(\frac{\pi\,\mu_n}{2}\right) + k, \tag{32}$$

represent the imaginary (dissipative) and real (conservative) portions of the system dynamics in response to incident radiation, respectively, and clearly $p_q = p_\zeta = (\mu_n, \gamma_n, m, c, k)$. The relationship between the stationary time domain model of (29)–(32) and the frequency domain model given in (22) and (23) is apparent by inspection. With this in mind, one observes that the frequency domain model represents a (continuously variable, data-dependent, stationary) Laplace transform of the data generating system assumed in (16) as well as any closed form linear ordinary differential model equation having a form such as (25). In other words, at every point, ν_m, in the modeled response band, the model (23) returns the Bode response (i.e.. the steady-state amplitude and phase response) of the media.

D. Steady-state response to radiative forcing

The steady-state response of the model (23) with respect to (17) is obtained by direct variable-order Laplace inversion using definition (5):

$$x_{ss}(t;\nu) = \lim_{t\uparrow\infty} \mathcal{L}^{-1}\{\zeta(\nu)^{-1} s^{-q(\nu)} \hat{F}(s)\},$$
$$= \lim_{t_0\downarrow-\infty} \frac{\nu^{q(\nu)}}{\zeta(\nu)} \int_{t_0}^{t} \frac{(t-\sigma)^{q(\nu)-1}}{\Gamma[q(\nu)]} F(\sigma)\, d\sigma, \qquad (33)$$

where $\mathcal{L}^{-1}\{\cdot\}$ is the inverse Laplace transform so that, assuming incident radiation $F(t;\lambda) = E_0\, \mathbb{R}\mathrm{e}\{\exp(i\, t/\lambda)\}$ having wavelength $\lambda = 1/\nu$, one obtains

$$\xi_{ss}(t;\nu) = \frac{\nu^{-q(\nu)}}{\zeta(\nu)} \cos\left[\nu\, t + \frac{\pi\, q(\nu)}{2}\right], \qquad (34)$$

where $\xi = x/E_0$. The result (34) clearly demonstrates that for such a system, the generalized differential order is directly coupled to the phase shift of the steady-state response. By comparison with Fig. 1, we see that a (hypothetical) purely conservative response results in either no phase shift or a 180° phase shift (depending on whether the system is elastic or inertial, respectively). A maximally dissipative response is one accompanied by a 90 degree phase shift, precisely as expected.

The steady-state response can also be written in terms of the displacement field D (i.e., accounting for the core polarizability) by consideration of (1):

$$\xi^D_{ss}(t;\nu) = \varepsilon_\infty \cos(\nu\, t) + \xi_{ss}(t;\, \nu). \qquad (35)$$

The accuracy of (34) and (35) is limited to the bandwidth of the experimental data.

E. Spectroscopic analysis with the VOF

1. Determination of the properties of the VOF by analysis of the CDHO over a range of damping values

The analytical value of the VOF is extended by considering the frequency response of the VOCs for a set of example systems. For the purposes of illustration, we define the sample set of CDHOs

$$\overline{\chi}^L(\nu) = \frac{1}{\nu_n^2 - \nu^2 + i\,\overline{\gamma}\,\nu}, \qquad (36)$$

where $\nu_n = \sqrt{2}$ and we let the damping take values on $\overline{\gamma} \in \{0.01, 0.5, 1, 1.5, 2, 2.5, 1000\}$, with the smallest and largest values representing the limiting cases $\overline{\gamma}/\nu_n \ll 1$ and $\overline{\gamma}/\nu_n \gg 1$, respectively. The remaining values have been selected to encompass a broad range of damping conditions with respect to the natural system dynamics: $\overline{\gamma}/\nu_n \lesssim 1$, $\overline{\gamma}/\nu_n \sim 1$, and $\overline{\gamma}/\nu_n \gtrsim 1$.

With $Z(\nu) = 1/\overline{\chi}^L(\nu)$, frequency-dependent and parametrically defined plots for the VOCs (22) corresponding to the set of response functions described by (36) are given in Fig. 2. By inspection of the plots, one immediately obtains the coefficient values for each system. Dynamics in the frequency response that are associated with the dominance of a particular term in the response function are represented by simultaneous flat bands in $q(\nu)$ and $\zeta(\nu)$, a property that will be leveraged further on when using the VOF to obtain parameters for a CD$^\mu$HO model using experimental data. The conditions of simultaneous VOC flat bands represents a more complete generalization of the properties noted by Jonscher during his investigations. For a true second-order system, this implies that the Hooke's law $q(\nu) \approx 0$ and Newton's law $q(\nu) \approx 2$ forces are associated with terms in all of the defined integer order response functions that can be described as dominant over a given band. This, of course, occurs at low and high frequencies for the order 0 and order 2 terms, respectively.

Only the function with $\overline{\gamma} = 1000$ produces a region of dominance for the order 1 term relative to the bandwidth of the response dynamics. Expanding on this point, one notes that the change in slope of q about the pivot point defined by $q(\nu_n) = 1$ has the following properties:

$$\lim_{\overline{\gamma}\downarrow 0} \left.\frac{dq}{d\nu}\right|_{\nu=\nu_n} = \infty, \qquad (37a)$$

$$\lim_{\overline{\gamma}\uparrow\infty} \left.\frac{dq}{d\nu}\right|_{\nu=\nu_n} = 0. \qquad (37b)$$

Condition (37a) describes first-order forces of null importance, whereas (37b) describes a system entirely dominated by viscous forces. More realistically, a first-order response due to arbitrarily large damping is represented by a nearly flat response over some dynamically relevant band, with q asymptoting to 0 at arbitrarily low frequencies and asymptoting to 2 at arbitrarily high frequencies. This is demonstrated in Fig. 2(a), where the dashed line is generated by the damping value $\overline{\gamma} = 1000$.

In other words—taking into account the behavior of q when order 0, 1, and 2 terms are important—the optimality bands (i.e., regions of flatness) in the q-ν plane suggest or correspond to discrete potentially interpolating terms in the system transfer function which define the system order over a given band. These tell us the spectral bands for which certain types of forces in the corresponding equations of motion (representing a force balance) become important. Furthermore, the pivot-slope behavior at $q(\nu_n) = 1$ demonstrates that the relative importance of an "interpolation order" at a given frequency corresponds to the instantaneous slope $dq/d\nu$, with shallower slopes implying greater importance.

2. Analysis of a Cole-Cole system with the VOF

As a final example, we consider dielectric relaxation in a non-Debye nanofluid that is well modeled by the Cole-Cole

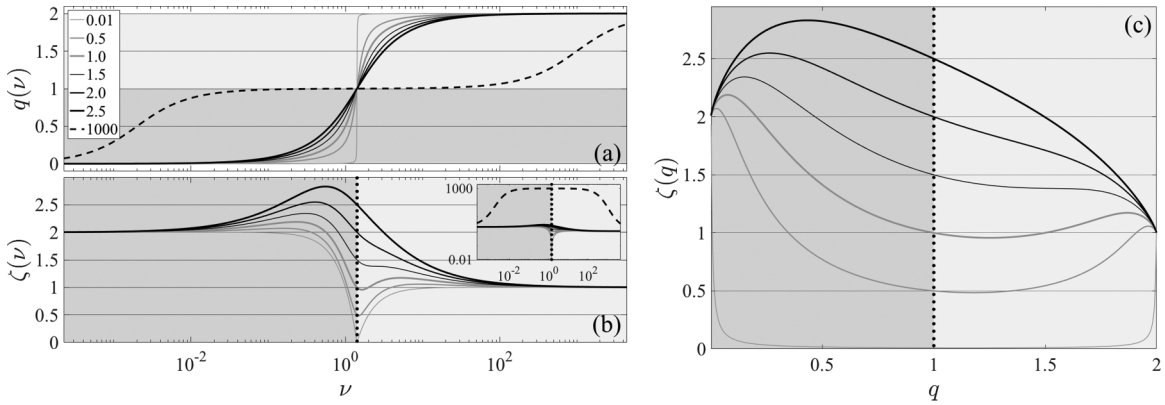

FIG. 2. Frequency response of the generalized differential order and generalized damping for a set of classical CDHOs (Lorentz oscillators), which correspond to second (integer) order displacement ODEs. The legend values correspond to the damping coefficients defining each system. The undamped natural frequency ν_n is indicated by the vertical dotted line in (b) and (c). Viscoelastic (viscoinertial) regimes are indicated by dark gray (light gray) regions, in accordance with the VOC diagram of Fig. 1. Simultaneous regions of relative flatness $dq/d\nu \approx 0$ and $d\zeta/d\nu \approx 0$ over a broad band indicate bandwidths for which a single term in the differential equation of motion dominates. For low ($\nu/\nu_n \ll 1$) and high ($\nu/\nu_n \gg 1$) frequencies, this will always lead to $q(\nu_{\text{low}}) \approx 0$ and $q(\nu_{\text{high}}) \approx 2$ (for a true second-order system), corresponding to Hooke's law (elastic) and Newton's law (inertial) forces, respectively. By comparison of (a) and the (log-log) inset of (b), it is clear that the system with very large damping has a dominating term over $\nu \in [10^{-2}, 10^{2}]$. Inspection of (a) reveals that $q(\nu_n) = 1$ (i.e., the differential order at the undamped natural frequency is 1). The coefficients for all terms in the system response function can be obtained by direct inspection of the generalized damping (b). In plot (c), the evolution of the generalized damping is plotted as a function of generalized differential order. The coefficients can be obtained by inspection of this plot as well.

equation. Systems such as these are often accurately captured by fractional differential descriptions due the memory effects imposed by viscoelastic transduction of the incident field [50]. The experimental data and corresponding Cole-Cole model, taken from Ref. [51], are for nanoparticles of graphene suspended in a squalene base fluid at a temperature of 343.15 K (70 °C). The parameters for the Cole-Cole model are: $\varepsilon_0 = 39.96$, $\varepsilon_\infty = 5.18$, $\tau = 856$ ns, and $\alpha = 0.28$. The fractional order in this model is then $\mu = 1 - \alpha = 0.72$. The generalized damping is asymptotically

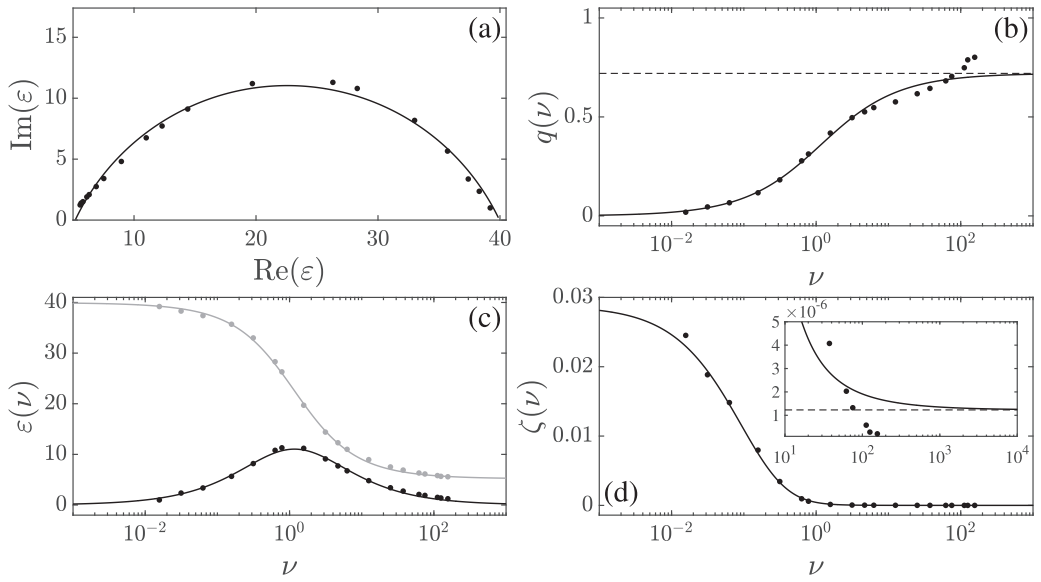

FIG. 3. Dielectric response of graphene nanoparticles dispersed in squalene at 343.15 K (70 °C). In each plot, the dots represent the experimental data and the lines represent the model. Both are taken from Ref. [51]. The plots of the real (gray) and imaginary (black) values for the dielectric function are given in (c). ν is given in units of MHz. In the Cole brothers' original derivation [39], the parameter α is related to the angle created by the offset of the semicircle origin from the $\mathbb{R}\text{e}\{\varepsilon\}$ axis (in the negative direction) in the Cole-Cole diagram for the dielectric function of (a). The parameters for the Cole-Cole model are: $\varepsilon_0 = 39.96$, $\varepsilon_\infty = 5.18$, $\tau = 856$ ns, and $\alpha = 0.28$. The fractional order in this model is then $\mu = 1 - \alpha = 0.72$, which is demonstrated by the dashed line in the $q(\nu)$ plot of (b). The generalized damping is asymptotically determined by the coefficients in the material response function: $1/(\varepsilon_0 - \varepsilon_\infty) = 0.0288$ at low frequencies and $\tau^\mu/(\varepsilon_0 - \varepsilon_\infty) \approx 1.23 \times 10^{-6}$ s$^\mu$ at high frequencies. The high-frequency asymptote is indicated by the dashed line in the inset of the $\zeta(\nu)$ plot of (d).

equivalent to: $1/(\varepsilon_0 - \varepsilon_\infty) = 0.0288$ at low frequencies and $\tau^\mu/(\varepsilon_0 - \varepsilon_\infty) \approx 1.23\times10^{-6}$ s$^\mu$ at high frequencies. In other words, the generalized damping provides (in this case) some measure of the evolution of the overall time constant of the response at a given forcing frequency, as determined by the coefficients of the material response function. The Cole-Cole diagram, the frequency-dependent dielectric function plot, and the VOC plots for the nanofluid are all given in Fig. 3. The plots demonstrate that the VOC framework provides the same meaningful interpretation for fractional systems as was demonstrated for integer order systems, regardless of whether inputs to the framework are in terms of a continuously defined model or in terms of discrete experimental data.

V. ANALYSIS OF THIN FILM RADIATIVE PHYSICS WITH THE VOF

We demonstrate here a "toy application" of the VOF to the estimation of the parameters for a single-oscillator response model for an IR absorption mode of SiO_2 using the CD$^\mu$HO as our model structure. For this purpose, we use the ellipsometric data of Ref. [46] obtained in tabular form from Ref. [47]. We consider the IR mode defined on $\nu \in [932, 6500]$ cm^{-1}. Our analysis is performed on a scaled grid $\underline{\nu}_m = k_\nu\, \nu_m$, where $k_\nu = \text{median}(\nu_m)^{-1}$ for the M-sized grid ν_m, $m \in [1, M]$, defined by the experimental data. As demonstrated in Ref. [52], this scaling gives better conditioning results than the inverse mean and is also the appropriate choice for use with models having a noninteger power-law grid dependence.

A. Obtaining a CD$^\mu$HO model from VOF analysis

The CD$^\mu$HO parameters are obtained by using the VOCs to estimate a portion of the dynamics and then subtracting the estimated dynamics from the experimental data. The VOCs are then used along with the unmodeled dynamics in order to estimate the remaining CD$^\mu$HO parameters. For this purpose, we use the model-fitting template

$$Z_m = \underline{a}_0 - \underline{a}_2\, \underline{\nu}_m^2 + \underline{a}_\mu (i\, \underline{\nu}_m)^\mu, \tag{38}$$

where $Z_m = \chi_m^{-1} = (\varepsilon_m - \varepsilon_\infty)^{-1}$ is the experimental data and the right-hand side of (38) is equivalent to the inverse of (9) under appropriate scaling and redefinition of the coefficients. The underbar notation indicates that the coefficients correspond to the scaled grid. We take $\varepsilon_\infty = 2.10$ from, e.g., Refs. [43,53].

The VOCs referenced in the following estimation procedure are ascertained by application of expressions (22) and can also be extracted from Fig. 4. Since our experimental data do not extend to a frequency where $q(\underline{\nu}_m) \approx 0$, allowing the estimation of $\underline{a}_0$, we begin with a unity DC gain assumption: $\underline{a}_0 = 1$. Deviation incurred by this assumption can be "scaled out" if needed after obtaining the remaining parameters. Then $\underline{a}_2 = \zeta(\underline{\nu}_{\text{high}}) \approx 19.22$, where $\underline{\nu}_{\text{high}} = k_\nu\, 6500 = 1.749$ is such that $q(\nu_{\text{high}}) \approx 2$.

In order to estimate the final set of parameters, we define the "unmodeled dynamics" as

$$\widetilde{Z}_m = Z_m - Z_0(\underline{\nu}_m), \tag{39}$$

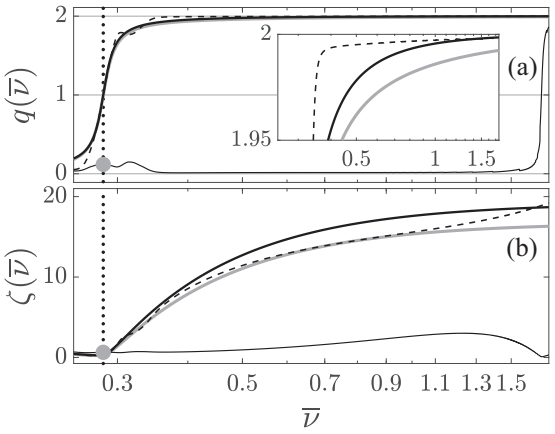

FIG. 4. VOCs for SiO_2 on the scaled grid $\underline{\nu} = k_\nu\, \nu$, where $\nu \in [932, 6500]$ cm^{-1}. Represented here are experimental data from Refs. [46,47] (dashed black line), an optimized CDHO (solid gray line), and the CD$^\mu$HO estimated using the VOF (thick solid black). The spectral coordinate for the maximum amplitude response is indicated by the vertical dotted line. The VOCs for the unmodeled dynamics $\widetilde{Z}$ are given by the thin solid line. The estimated damping parameters (at resonance) are indicated in each plot with a gray dot. Comparison of expression (34) for the steady-state radiative response with the improved tracking of the generalized differential order provided by the CD$^\mu$HO in the inset of (a) reveals that the fractional model will provide better phase reproduction at higher frequencies.

where $Z_0(\underline{\nu}_m) = \underline{a}_0 - \underline{a}_2\, \underline{\nu}_m^2$ are the dynamics that have already been estimated. In other words, Z_0 contains the low- and high-frequency dynamics, which represent the elastic and inertial conservative portions, respectively. Noting the results of our previous analysis—that the interpolated damping is innately expressed at the natural frequency—we can use the remaining unmodeled dynamics $\widetilde{Z}_m$ with the VOCs to estimate the remaining parameters. The natural frequency is taken to be that of the maximum susceptibility, $\underline{\nu}_n \approx \underline{\nu}_r = k_\nu\, 1052 = 0.2831$. Here $\underline{\nu}_r = k_\nu\, \nu_r$, where ν_r is the resonant (or maximum amplitude response) frequency. Note that in general, $\nu_n \neq \nu_r$ for any system with nonzero damping, but the two are approximately equivalent when $\gamma/\nu_n \ll 1$. Our remaining estimated parameters are then $\mu = q(\widetilde{Z}(\underline{\nu}_r)) = 0.12$ and $\underline{a}_\mu = \zeta(\widetilde{Z}(\underline{\nu}_r)) = 0.64$.

The final estimation step, along with the resulting estimated VOCs, are shown in Fig. 4. Also shown in the figure is a traditional integer order CDHO with parameters obtained by optimization: $\nu_p = 909.86$, $\gamma = 75.39$, and $\nu_n = 1052.26$. A closer inspection of the unmodeled dynamics $\widetilde{Z}_m$ is provided in Fig. 5, where the $\underline{\nu}$ axis has been "zoomed in" to the range covering the primary response dynamics. Over this range, the VOCs remain approximately constant—a condition that is analogous to Jonscher's result (24)—which suggests that the remaining damping term can be modeled with a fractional term. A subtle-yet-important detail expressed in the figure is the fact that, although the resulting CD$^\mu$HO has utilized this noninteger order damping term, it nonetheless attains $q(\underline{\nu}_n) = q(\nu_n) = 1$. This is consistent with the experimental data and with the CDHO.

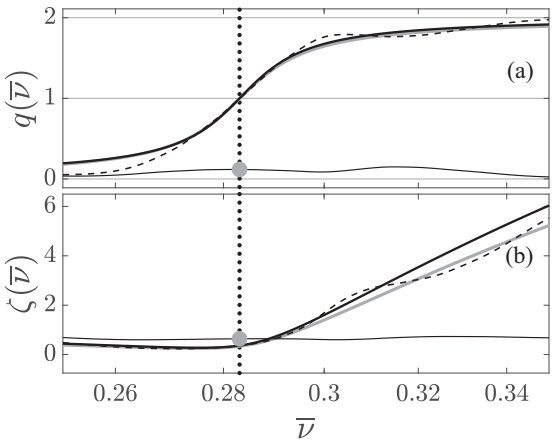

FIG. 5. The same as in Fig. 4, except "zoomed in" to the bandwidth of the primary response dynamics. In the unscaled grid, this range is equivalent to $\nu \in [932, 1300]$ cm^{-1}. The unmodeled dynamics are approximately constant with respect to frequency over the dynamic bandwidth and—in accordance with the analysis properties described in Sec. IV E 1—suggest a damping term having noninteger generalized differential order $\mu = q \approx 0.12$ and corresponding generalized damping $\zeta \approx 0.64$ over this band. Despite the nonlocal damping term in the obtained CD$^{\mu}$HO model, the generalized differential order nonetheless attains $q(\underline{\nu}_n) = q(\nu_n) = 1$, thus retaining the property of maximal dissipation at resonance, in agreement with the CDHO and the experimental data.

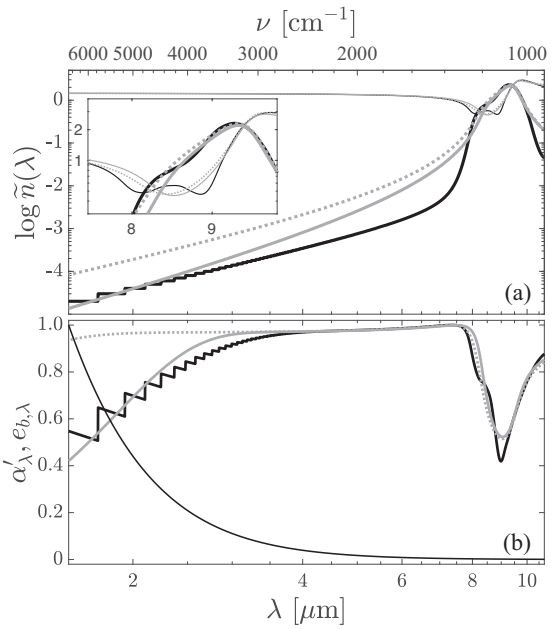

FIG. 6. Optical and radiative characteristics of the midinfrared response of SiO_2. (a) Dispersive (thin lines) and absorptive (thick lines) indices for the experimental data [46,47] (solid black), CDHO (dashed gray), and CD$^{\mu}$HO (solid gray). (b) Spectral normal absorptivity computed from corresponding complex refractive indices in the top plot. The thin black line is Planck's distribution (normalized) for a black body emitter assuming approximate equivalent temperature of the Sun $T_\odot \approx 5785$ K. The CD$^{\mu}$HO has better reproduction of the generalized differential order at smaller wavelengths [see Fig. 4(a)], which corresponds to the improved tracking of the absorption index in the attenuation band $\lambda \lesssim 4$ μm. In contrast, the CDHO is unable to accurately reproduce this behavior, leading to substantial overestimation of the absorption at smaller wavelengths. Integration over Planck's distribution during computation of the total absorptivity significantly augments the accumulated error.

The fundamental difference between the CD$^{\mu}$HO and the CDHO is that the former (within the present context) will more accurately model the attenuated high-frequency dynamics. This is primarily due to the improved high-frequency phase-matching behavior of the CD$^{\mu}$HO. Recalling our earlier discussion relating the generalized differential order q to the phase of the steady-state radiative response (34), this improved phase matching can be observed in the inset of the $q(\underline{\nu})$ analysis plot of Fig. 4. As we show presently, this feature has important implications for the estimation of bulk radiative properties.

Once obtained on the scaled grid, the estimated CD$^{\mu}$HO parameters are rescaled to the original grid as described in Ref. [52]. After rescaling, they are (in units of cm^{-1}): $\nu_p = (1/a_2)^{1/2} \approx 848$, $\gamma_\mu = (a_\mu/a_2)^{1/\overline{\mu}} \approx 608$, and $\nu_\mu = (a_0/a_2)^{1/2} \approx 848$, where $\overline{\mu} = 2 - \mu$ with $\mu = 0.12$.

B. Estimation of absorptivity using VOF results

Let us now consider the optical response of a thin film of amorphous silicon dioxide having uniform thickness $h = 5$ mm. Following the analysis of Ref. [24], we consider the spectral normal absorptivity α'_λ of the film in the presence of normally incident radiation:

$$\alpha'_\lambda = \frac{(1 - \mathscr{R}_n)(1 - \mathscr{T}_{\text{film}})}{1 - \mathscr{R}_n \mathscr{T}_{\text{film}}}, \tag{40}$$

where the normal interface reflectivity is

$$\mathscr{R}_n = \frac{(n-1)^2 + k^2}{(n+1)^2 + k^2}, \tag{41}$$

and the internal film transmittance is

$$\mathscr{T}_{\text{film}} = \exp\left(-\frac{4\pi k h}{\lambda}\right), \tag{42}$$

for incident radiation having wavelength λ. One can then estimate the total normal absorptivity of the film along this band when exposed to, e.g., solar radiation by integration over Planck's energy density distribution for an ideal blackbody emitter [54]

$$e_{b,\lambda} = \frac{C_1}{\lambda^5[\exp(C_2/\lambda T_\odot) - 1]}, \tag{43}$$

where $T_\odot \approx 5785$ K is an approximate equivalent temperature for the Sun. Here $C_1 = 2\pi h_P c_0^2$ and $C_2 = h_P c_0/k_B$, with h_P being Planck's constant, k_B being Boltzmann's constant, and where c_0 is the speed of light in a vacuum.

The complex refractive index and the spectral normal absorptivity for the data and models have been plotted in Fig. 6. Displayed alongside the absorptivity is Planck's distribution (normalized to its corresponding maximum). The CDHO does not accurately track the absorption index in the high-frequency attenuation band. This translates to a factor of 2 overestimation of the spectral absorptivity at small

wavelengths. The mean absolute percentage error for the CDHO estimation of the spectral absorptivity is ≈24%, while for the CD$^{\mu}$HO it is just under 5%. Due to the significant weighting imposed by Planck's distribution at small wavelengths (where the model mismatch is the greatest), the CDHO overestimates the total absorptivity by ≈33%. The CD$^{\mu}$HO, on the other hand, underestimates the total absorptivity by just 0.35%, representing two orders of magnitude improvement over the integer order model.

C. Estimation of absorptivity by optimization

Assessing the aptitude of the foregoing approximate method for producing a reasonably accurate spectral model of the material absorptivity (within the CD$^{\mu}$HO model structure) entails comparing the results against those obtained from an optimal configuration. This, however, is not a straightforward task. This is because the VOF method has produced a CD$^{\mu}$HO model having fidelity in two different spaces: that of the complex refractive index and that of the absorptivity. The complication arises when forming the standard data-fitting objective for such a problem:

$$\mathcal{V}(\theta) = \sum_{m=1}^{M} S(\nu_m; \theta), \tag{44}$$

where S is the weighted power spectrum for the model mismatch

$$S(\nu_m; \theta) = (\psi_r(\nu_m)\,|\Delta_r(\nu_m; \theta)|)^2 + (\psi_i(\nu_m)\,|\Delta_i(\nu_m; \theta)|)^2, \tag{45}$$

and the mismatch terms being minimized are

$$\Delta_r(\nu_m; \theta) = \chi'(\nu_m; \theta) - \chi'_m, \tag{46a}$$

$$\Delta_i(\nu_m; \theta) = \chi''(\nu_m; \theta) - \chi''_m. \tag{46b}$$

Here $\chi(\nu; \theta) = \chi'(\nu; \theta) - i\,\chi''(\nu; \theta)$ is the respective model evaluated at a frequency ν given a parameter set θ, and $\chi_m = \chi'_m - i\,\chi''_m$ is the experimental data defined on the M-sized frequency grid, ν_m, $m \in [1, M]$.

The frequency-dependent weightings $\psi_r(\nu_m)$ and $\psi_i(\nu_m)$ are chosen depending on the intended application [55]. For a reasonably accurate fit to the most important, nonattenuated features of the refractive indices, one would assume that the weightings $\psi_r = \psi_i = 1$ are sufficient. However, by comparing the refractive indices with the spectral absorptivity (as in Fig. 6), it is clear that the attenuated region at smaller wavelengths also becomes important when an accurate model is needed for the spectral absorptivity. Furthermore, with respect to Fig. 6 one observes that the important (nonattenuated) regions of the refractive indices and the unimportant (highly attenuated) regions of the refractive indices carry the reverse significance when the model is used to compute the *total* absorptivity by integrating over Planck's distribution.

To mitigate issues resulting from the disparity between attenuated and nonattenuated regions in spectroscopic data, it is typical to define weightings having the form $\psi_r(\nu_m) = 1/|\chi'_m|$ and $\psi_i(\nu_m) = 1/|\chi''_m|$. This approach is insufficient in the present setting, since it will tend to overemphasize the attenuated regions, leading to models that do not reproduce to sufficient accuracy the dynamics near resonance. Rather than resorting to the complications of a multiobjective optimization setting, we note that the particular form of the spectral absorptivity (or of similar radiative properties) is such that it can be exploited to embed the secondary objective into (44) by choosing the weightings

$$\psi_r(\nu_m) = \psi_i(\nu_m) = 1/\alpha'_\lambda(\nu_m). \tag{47}$$

The reason why this is expected to yield desirable results is made evident by inspection of Fig. 6. In particular, with respect to (40), (41), and (42), regions having little effect in determining the spectral absorptivity receive the weighting $1/\alpha'_{\max} \approx 1$ when $\alpha'_{\max}$ is close to unity. Those playing a more important role receive the weighting $1/\bar{\alpha}' > 1$ where $\bar{\alpha}' < \alpha'_{\max} \leqslant 1$. In other words, mismatch having little effect is "left alone" while that playing a larger role is emphasized during optimization. A comparison of various spectral weighting strategies is demonstrated in Fig. 7.

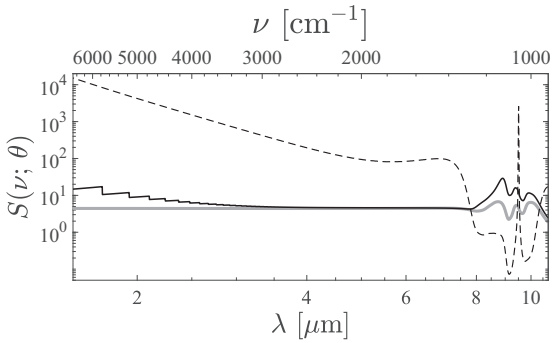

FIG. 7. Weighted power spectra for the model mismatch. Each line represents error at the outset of an optimization algorithm, initialized with the optimal CDHO configuration. The thick solid gray line represents no weighting of the error terms, the thin dashed gray line represents error weighted by the data (i.e., relative error), and the thin solid black line is the error weighted by the inverse spectral normal absorptivity. The inverse absorptivity emphasizes only the relevant regions and does so in a smooth, continuous manner. The relative error weighting tends to overemphasize attenuated regions and deemphasize dynamics near resonance.

Since the spectral absorptivity is a continuously defined function of frequency (or wavelength) that is relevant to the physics of the problem and which also considers the thickness of the film directly via (42), the smoothly modified optimization problem yields the desired multiobjective result, but does so without inflating the cardinality of the nonconvex optimization space (as would likely be the case with a traditional multiobjective formulation). By fixing the values of μ on the domain $\mu \in (0, 2)$ with a step size of $\Delta\,\mu = 0.01$, and then optimizing the CD$^{\mu}$HO at each of these values, the Pareto front in Fig. 8 was obtained.

Of the numerous conclusions that can be drawn from such a plot, we highlight three here. First, one notes that properly weighting the problem has little effect on the performance of the integer order CDHO model. This is, of course, due to the fact that it is constrained to integer order grid dependence, and accurately reproducing both the spectral absorptivity and the refractive index requires capturing the attenuated dynamics without incurring mismatch in the vicinity of resonance. The

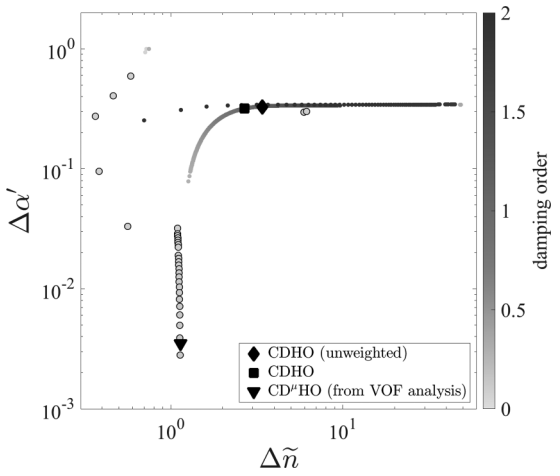

FIG. 8. Pareto optimality for minimization of model mismatch in the space of the refractive indices and the total normal absorptivity. Here $\Delta\widetilde{n}$ is the relative root mean squared error of the complex refractive index and $\Delta\alpha'$ is the mean absolute relative error of the total normal absorptivity. Models were optimized using the inverse spectral absorptivity to weight the error terms in the objective. The optimality is characterized over the entire range of KKR-compliant damping orders, $\mu \in (0, 2)$, with a step size of $\Delta\mu = 0.01$. The larger circular markers with thin black outlines indicate models defined on $\mu \in [0.07, 0.13]$, a range which evidently has a distinct fidelity in the multiobjective setting. The Pareto front consists entirely of a subset of this range. The indicator for the CDHO represents the optimal CD$^\mu$HO configuration with μ fixed to unity.

second note of import is that the entire Pareto front constitutes the subset with $\mu \in [0.07, 0.13]$, which is a range of μ yielding a fidelity that is distinct from other values. Our final important conclusion is that the CD$^\mu$HO configuration obtained by means of the VOF analysis very nearly achieves the point on the Pareto front yielding the best combined results for the refractive index and the absorptivity (as determined by a Euclidean measure).

VI. CONCLUDING REMARKS

Over the last few decades, nonlocal (i.e., fractional and variable-order) differential and integral operators have received an increasing level of attention from both researchers and practitioners due to their utility when modeling anomalous responses that may arise as the result of many-body dynamics. Reproducing such effects is often an intractable task for models utilizing local (i.e., integer order) operators alone, as these effects manifest from a dynamical scale approaching "infinite dimensionality." Under amenable conditions, describing behaviors in this space with closed-form models possessing parsimonious parametrizations therefore entails the use of nonlocal operators. This is because they possess the requisite inherent infinite dimensionality.

A significant demand is placed on the acuity of the user when first encountering the differintegral time domain expressions that define temporally nonlocal operators. This is due to complications that inevitably arise from attempting to reconcile their meaning (mathematical or physical) with the intuitions established during the study of the integer order calculus. In a stationary frequency domain setting, however, interpreting temporally nonlocal operators is a more straightforward mathematical endeavor that also lends itself well to physical interpretation. This interpretation can be directly extended to linear combinations of such operators—resulting from a set of corresponding linear differential equations of motion—and to the systems they describe.

In this work, a generalized, variable-order framework (or formalism), denoted VOF, has been derived for the analysis and interpretation of complex frequency domain data. The framework has been extended for use with spectroscopic systems. These systems provide a natural setting for this generalized analysis since they possess the pertinent characteristics: they are defined by many-body dynamics, they are characterized by the dispersion of energy, and they are innately described by a complex-valued response function of frequency (or wavelength). It has been demonstrated that the VOF represents a generalization of other related mathematical descriptions such as the Cole-Cole equation and Jonscher's well-known "universal dielectric response" theory.

To facilitate a practical application of the VOF (i.e., beyond interpretive analysis), a nonlocal generalization of the classical Lorentz harmonic oscillator has been defined. The generalized model, denoted CD$^\mu$HO, represents the (complex-valued) frequency response function corresponding to a time domain fractional differential equation of motion where the emergent dissipative damping term may have a historical path dependence on particle-field interactions. This generalization is, in its essence, analogous to the manner in which the Cole-Cole equation generalizes the Debye theory.

An example application has been demonstrated for the determination of the parameters for a CD$^\mu$HO model of the midinfrared susceptibility of amorphous quartz silica (SiO_2). With the use of the resulting modeled absorptive-dispersive indices, an estimate for the spectral normal absorptivity has been obtained. The fidelity of the model obtained using the VOF has been compared with that obtained within a multiobjective setting (in terms of the refractive indices and the absorptivity).

The CD$^\mu$HO model obtained by VOF analysis demonstrates a fidelity very near that of the point on the Pareto front yielding the lowest combined error for the refractive indices and the total absorptivity. The results of the optimization also reveal the existence of a specific well-defined region of nonlocality having a distinct fidelity within the prescribed multiobjective space. It has been shown that this fidelity is inaccessible when an integer order description is employed.

APPENDIX: GENERALIZED DIFFERENTIAL OPERATOR

Starting with the variable-order differential operator originally proposed in Ref. [15]:

$$ {}_*\mathcal{D}^{q(t)}x(t) = \frac{1}{\Gamma[1-q(t)]}\int_{t_{0+}}^{t}(t-\sigma)^{-q(t)}\mathcal{D}^1 x(\sigma)\,d\sigma + \frac{[x(t_{0^+}) - x(t_{0^-})]\,t^{q(t)}}{\Gamma[1-q(t)]}, $$

which is valid for $q(t) < 1$, and performing sequential integration by parts to shift the indetermination caused by

the gamma function in the denominator, it is relatively straightforward to move the indetermination caused by a zero-valued denominator by shifting the argument of the gamma function to a generic integer value $M > q(t)$. By doing so we arrive at Coimbra's generalized order differential operator [25]:

$$ {}_{C}\mathcal{D}^{q(t)}x(t) = \frac{1}{\Gamma[M-q(t)]}\int_{0+}^{t}(t-\sigma)^{M-1-q(t)}\mathcal{D}^{M}x(\sigma)\,d\sigma + \sum_{m=0}^{M-1}\frac{[\mathcal{D}^{m}x(t_{0^+})-\mathcal{D}^{m}x(t_{0^-})]\,t^{m-q(t)}}{\Gamma[m+1-q(t)]}, $$

which is now valid for any value $q(t) < M$. The value of the next larger integer M can be arbitrarily chosen as long as $x(t)$ is differentiable to commensurate order.

Note that the last (summation) term in the generalized operator above can be reexpressed as

$$ \sum_{m=0}^{M-1}\frac{[\mathcal{D}^{m}x(t_{0^+})-\mathcal{D}^{m}x(t_{0^-})]t^{m-q(t)}}{\Gamma[m+1-q(t)]} = \frac{1}{\Gamma[M-q(t)]}\sum_{m=0}^{M-1}\left\{[\mathcal{D}^{m}x(t_{0^+})-\mathcal{D}^{m}x(t_{0^-})]\;t^{m-q(t)}\prod_{j=m+1}^{M-1}[j-q(t)]\right\}, $$

in order to keep the denominator in the positive branch of the gamma function. This yields a more desirable form from the viewpoint of practical numerical evaluation.

[1] K. S. Miller and B. Ross, *An Introduction to the Fractional Calculus and Fractional Differential Equations* (Wiley, New York, 1993).

[2] J. Sabatier, M. Aoun, A. Oustaloup, G. Grégoire, F. Ragot, and P. Roy, Fractional system identification for lead acid battery state of charge estimation, Signal Process. **86**, 2645 (2006).

[3] T. J. Anastasio, The fractional-order dynamics of brainstem vestibulo-oculomotor neurons, Biol. Cybern. **72**, 69 (1994).

[4] C. F. M. Coimbra, D. L'Espérance, R. A. Lambert, J. D. Trolinger, and R. H. Rangel, An experimental study on stationary history effects in high-frequency Stokes flows, J. Fluid Mech. **504**, 353 (2004).

[5] J. Boksiner and P. L. Leath, Dielectric breakdown in media with defects, Phys. Rev. E **57**, 3531 (1998).

[6] V. Tramontana, G. Casasanta, R. Garra, and A. M. Iannarelli, An application of Wright functions to the photon propagation, J. Quant. Spectrosc. Radiat. Transfer **124**, 45 (2013).

[7] S. Westerlund, Dead matter has memory! Phys. Scr. **43**, 174 (1991).

[8] M. Kh. Salakhov, An algorithm for the differentiation of arbitrary order in the solution of inversion problems in applied spectroscopy, J. Quant. Spectrosc. Radiat. Transfer **42**, 635 (1989).

[9] M. Caputo and F. Mainardi, A new dissipation model based on memory mechanism, Pure Appl. Geophys. **91**, 134 (1971).

[10] F. Mainardi, *Fractional Calculus and Waves in Linear Viscoelasticity: An Introduction to Mathematical Models* (Imperial College Press, London, 2010).

[11] P. J. Torvik and R. L. Bagley, On the appearance of the fractional derivative in the behavior of real materials, J. Appl. Mech. **51**, 294 (1984).

[12] S. G. Samko and B. Ross, Integration and differentiation to a variable fractional order, Integr. Transf. Spec. F **1**, 277 (1993).

[13] B. Ross and S. Samko, Fractional integration operator of variable order in the Hölder spaces $H^{\lambda(x)}$, Intl. J. Math. Math. Sci. **18**, 777 (1995).

[14] C. F. Lorenzo and T. T. Hartley, Variable order and distributed order fractional operators, Nonlinear Dyn. **29**, 57 (2002).

[15] C. F. M. Coimbra, Mechanics with variable-order differential operators, Ann. Phys. **12**, 692 (2003).

[16] L. E. S. Ramirez and C. F. M. Coimbra, On the selection and meaning of variable order operators for dynamic modeling, Int. J. Differ. Equ. **2010**, 846107 (2010).

[17] L. E. S. Ramirez and C. F. M. Coimbra, A variable order constitutive relation for viscoelasticity, Ann. Phys. **16**, 543 (2007).

[18] H. Zhang, F. Liu, P. Zhuang, I. Turner, and V. Anh, Numerical analysis of a new space–time variable fractional order advection–dispersion equation, Appl. Math. Comput. **242**, 541 (2014).

[19] H. T. C. Pedro, M. H. Kobayashi, J. M. C. Pereira, and C. F. M. Coimbra, Variable order modeling of diffusive-convective effects on the oscillatory flow past a sphere, J. Vib. Control **14**, 1659 (2008).

[20] L. E. S. Ramirez and C. F. M. Coimbra, On the variable order dynamics of the nonlinear wake caused by a sedimenting particle, Physica D **240**, 1111 (2011).

[21] J. Orosco and C. F. M. Coimbra, On the control and stability of variable-order mechanical systems, Nonlinear Dyn. **86**, 695 (2016).

[22] P. Grigolini, A. Rocco, and B. J. West, Fractional calculus as a macroscopic manifestation of randomness, Phys. Rev. E **59**, 2603 (1999).

[23] A. A. Stanislavsky, Memory effects and macroscopic manifestation of randomness, Phys. Rev. E **61**, 4752 (2000).

[24] M. Quinn Brewster, *Thermal Radiative Transfer and Properties* (John Wiley & Sons, New York, 1992).

[25] C. F. M. Coimbra, Methods of using generalized order differentiation and integration of input variables to forecast trends, U.S. Patent Application 13,641,083 (2013).

[26] C. M. Soon, C. F. M. Coimbra, and M. H. Kobayashi, The variable viscoelasticity oscillator, Ann. Phys. **14**, 378 (2005).

[27] N. W. Ashcroft and N. David Mermin, *Solid State Physics* (CBS Publishing Asia, Philadelphia, 1976).

[28] S. H. Simon, *The Oxford Solid State Basics* (Oxford University Press, Oxford, 2016).

[29] M. Dressel and G. Grüner, *Electrodynamics of Solids: Optical Properties of Electrons in Matter* (Cambridge University Press, Cambridge, 2002).

[30] Y. Mishin and J. Hickman, Energy spectrum of a Langevin oscillator, Phys. Rev. E **94**, 062151 (2016).
[31] H. W. Sheng, W. K. Luo, F. M. Alamgir, J. M. Bai, and E. Ma, Atomic packing and short-to-medium-range order in metallic glasses, Nature (London) **439**, 419 (2006).
[32] S. Burov and E. Barkai, Fractional Langevin equation: Overdamped, underdamped, and critical behaviors, Phys. Rev. E **78**, 031112 (2008).
[33] I. Podlubny, *Fractional Differential Equations*, *Mathematics in Science and Engineering* Vol. 198 (Academic Press, San Diego, 1999).
[34] L. Ferialdi and D. Dürr, Effective non-Markovian description of a system interacting with a bath, J. Math. Phys. **57**, 062101 (2016).
[35] Z. Sun, H. Dong, and Y. Zheng, Fractional dynamics using an ensemble of classical trajectories, Phys. Rev. E **97**, 012132 (2018).
[36] A. K. Jonscher, The "universal" dielectric response, Nature (London) **267**, 673 (1977).
[37] A. B. Basset, On the motion of a sphere in a viscous liquid, Philos. Trans. R. Soc. Lond. A **179**, 43 (1888).
[38] G. Casasanta, D. Ciani, and R. Garra, Non-exponential extinction of radiation by fractional calculus modeling, J. Quant. Spectrosc. Radiat. Transfer **113**, 194 (2012).
[39] K. S. Cole and R. H. Cole, Dispersion and absorption in dielectrics I. Alternating current characteristics, J. Chem. Phys. **9**, 341 (1941).
[40] H. A. Kramers, La diffusion de la lumière par les atomes, in *Atti del Congresso Internazionale dei Fisici* (N. Zanichelli, Bologna, 1927), Vol. 2, pp. 545–557.
[41] R. de L. Kronig, On the theory of dispersion of x-rays, J. Opt. Soc. Am. **12**, 547 (1926).
[42] V. Lucarini, K.-E. Peiponen, J. J. Saarinen, and E. M. Vartiainen, *Kramers-Kronig Relations in Optical Materials Research*, Springer Series in Optical Sciences Vol. 110 (Springer, Berlin, 2005).
[43] J. Orosco and C. F. M. Coimbra, Optical response of thin amorphous films to infrared radiation, Phys. Rev. B **97**, 094301 (2018).
[44] S. Lang, *Complex Analysis*, 4th ed. (Springer, New York, 1999).
[45] F. Wooten, *Optical Properties of Solids* (Academic Press, New York, 1972).
[46] J. Kischkat, S. Peters, B. Gruska, M. Semtsiv, M. Chashnikova, M. Klinkmüller, O. Fedosenko, S. Machulik, A. Aleksandrova, G. Monastyrskyi, Y. Flores, and W. T. Masselink, Mid-infrared optical properties of thin films of aluminum oxide, titanium dioxide, silicon dioxide, aluminum nitride, and silicon nitride, Appl. Opt. **51**, 6789 (2012).
[47] M. N. Polyanskiy, Refractive index of SiO_2 (silicon dioxide, silica, quartz), Kischkat, https://refractiveindex.info/cite.php.
[48] V. De Grandis, P. Gallo, and M. Rovere, Computer simulation of the phase diagram for a fluid confined in a fractal and disordered porous material, Phys. Rev. E **70**, 061505 (2004).
[49] V. Raicu, Dielectric dispersion of biological matter: Model combining Debye-type and "universal" responses, Phys. Rev. E **60**, 4677 (1999).
[50] R. F. Rodríguez, J. Fujioka, and E. Salinas-Rodríguez, Fractional fluctuation effects on the light scattered by a viscoelastic suspension, Phys. Rev. E **88**, 022154 (2013).
[51] T. P. Iglesias, G. Vilão, and J. C. R. Reis, An approach to the interpretation of Cole-Davidson and Cole-Cole dielectric functions, J. Appl. Phys. **122**, 074102 (2017).
[52] R. Pintelon and I. Kollár, On the frequency scaling in continuous-time modeling, IEEE T. Instrum. Meas. **54**, 318 (2005).
[53] S. I. Popova, T. S. Tolstykh, and V. T. Vorobev, Optical characteristics of amorphous quartz in the 1400–200-cm^{-1} region, Opt. Spectrosc. **33**, 444 (1972).
[54] S. S. Penner, *Quantitative Molecular Spectroscopy and Gas Emissivities* (Addison-Wesley, Reading, MA, 1959).
[55] J. Orosco and C. F. M. Coimbra, On a causal dispersion model for the optical properties of metals, Appl. Opt. **57**, 5333 (2018).